



## OPEN ACCESS

## EDITED BY

Cédric Jamet,  
UMR8187 Laboratoire d'Océanologie et de  
Géosciences (LOG), France

## REVIEWED BY

Robert J. Frouin,  
University of California, San Diego,  
United States  
Agnieszka Bialek,  
National Physical Laboratory, United Kingdom

## \*CORRESPONDENCE

Catherine Mitchell

✉ [cmitchell@bigelow.org](mailto:cmitchell@bigelow.org)

RECEIVED 08 October 2024

ACCEPTED 12 February 2025

PUBLISHED 05 March 2025

## CITATION

Shunmugapandi R, McCarry CL, McKee D and  
Mitchell C (2025) Ocean color anomaly  
detection to estimate surface *Calanus*  
*finmarchicus* concentration in  
the Gulf of Maine.

*Front. Mar. Sci.* 12:1507638.

doi: 10.3389/fmars.2025.1507638

## COPYRIGHT

© 2025 Shunmugapandi, McCarry, McKee and  
Mitchell. This is an open-access article  
distributed under the terms of the [Creative  
Commons Attribution License \(CC BY\)](https://creativecommons.org/licenses/by/4.0/). The  
use, distribution or reproduction in other  
forums is permitted, provided the original  
author(s) and the copyright owner(s) are  
credited and that the original publication in  
this journal is cited, in accordance with  
accepted academic practice. No use,  
distribution or reproduction is permitted  
which does not comply with these terms.

# Ocean color anomaly detection to estimate surface *Calanus finmarchicus* concentration in the Gulf of Maine

Rebekah Shunmugapandi<sup>1</sup>, Cait L. McCarry<sup>1</sup>, David McKee<sup>2,3</sup>  
and Catherine Mitchell<sup>1\*</sup>

<sup>1</sup>Bigelow Laboratory for Ocean Sciences, East Boothbay, ME, United States, <sup>2</sup>University of Strathclyde, Glasgow, United Kingdom, <sup>3</sup>University of the Arctic in Tromsø, Tromsø, Norway

The planktonic copepod, *Calanus finmarchicus*, plays a pivotal role in the Gulf of Maine (GoM) pelagic food web as a primary food source for many species, including the critically endangered North Atlantic right whale (NARW). Thus, observing *C. finmarchicus* on a Gulf-wide scale via satellite could be beneficial for understanding changes in the migration patterns of the NARW. This study investigated the application of ocean color remote sensing to detect the surface population levels of *C. finmarchicus* in the GoM. Using remote sensing reflectance data from the MODIS Aqua sensor, we processed enhanced RGB (eRGB) imagery to detect and quantify the presence of *C. finmarchicus*, which is identifiable by its red astaxanthin pigment. This study employed a refined approach from the method originally developed off the coast of Norway, which integrates eRGB imagery and radiative transfer modeling to generate optical anomaly maps that are used for quantifying surface *C. finmarchicus* concentrations in the GoM. We detected surface swarms of *C. finmarchicus* in the ocean color imagery and estimated their concentrations. However, due to the method's reliance on astaxanthin/red pigment-based detection, other astaxanthin-rich red/brown plankton were misidentified as *C. finmarchicus*. While the approach presented is effective for identifying astaxanthin anomalies in ocean color and holds potential for quantifying the surface populations of *C. finmarchicus*, it requires local knowledge to accurately quantify the *C. finmarchicus* abundances.

## KEYWORDS

*Calanus finmarchicus*, zooplankton, ocean color, satellite remote sensing, Gulf of Maine

## 1 Introduction

Ocean color remote sensing has significantly advanced the monitoring of optically significant constituents (OSCs) in marine ecosystems, allowing for consistent, wide-scale observation of marine ecosystems, which has enhanced our understanding of the ocean environment over time and space (Groom et al., 2019). The core of ocean color remote

sensing relies on understanding the interactions between light and OSCs in the water. These OSCs have distinct properties for absorbing and scattering light, which influences how light behaves in the marine environment (Dierssen and Randolph, 2013; Mascarenhas and Keck, 2018). Traditionally, OSCs are classified into three main groups: phytoplankton, colored dissolved organic matter (CDOM), and non-algal/inorganic particles (NAPs) (Dierssen and Randolph, 2013; Werdell et al., 2018). However, recent work has shown that the presence of pigments in organisms other than phytoplankton can also alter the optical characteristics of water, specifically the zooplankton *Calanus finmarchicus* (Basedow et al., 2019; McCarry et al., 2023).

*C. finmarchicus* is a lipid-rich calanoid copepod that is dominant in the Gulf of Maine (GoM) (Bigelow, 1926; Johnson et al., 2011; Ji et al., 2022). It is recognized as a foundation of the GoM pelagic food web by transferring primary production to higher-level consumers (Grieve et al., 2017; Renaud et al., 2018; Melle et al., 2014). *C. finmarchicus* is particularly important, as it forms the primary food source for the critically endangered planktivorous North Atlantic right whale (NARW) (Ross et al., 2023; Swaim et al., 2009; Michaud and Taggart, 2007). The NARW population is experiencing an increased mortality rate, with population numbers decreasing to less than 360 individuals in the last decade (Meyer-Gutbrod et al., 2021; Moore et al., 2021). The migration and calving rate of the NARW in the GoM are influenced by the availability of *C. finmarchicus* (Sorochan et al., 2021). Changes in the distribution of *C. finmarchicus* affect the migratory and distribution patterns of NARW (Record et al., 2019; Meyer-Gutbrod et al., 2021). Therefore, monitoring of *C. finmarchicus* is important for tracking and predicting the movement of NARW. Traditional shipboard and buoy methods of assessing *C. finmarchicus* abundance cannot provide continuous regional monitoring and are limited in scope for mapping spatial distribution; therefore, satellite observations could fill a gap in current observation strategies.

*C. finmarchicus* is often referred to as “red feed”; it synthesizes a red carotenoid, astaxanthin, from precursor pigments through its algal diet (Byron, 1982; Matsuno, 2001; Vilgrain et al., 2023). Due to this pigmentation, surface waters can appear red when *C. finmarchicus* is swarming (Basedow et al., 2019). These red surface swarms significantly influence the optical properties of water and are captured by satellite (Basedow et al., 2019; McCarry et al., 2023). Furthermore, *C. finmarchicus* concentrations have been estimated from satellite ocean color data for a swarm off the coast of Norway (McCarthy et al., 2023). Thus, detecting the movement and quantifying the surface abundance of *C. finmarchicus* in the GoM using ocean color remote sensing could help track *C. finmarchicus* on a regional scale and aid in monitoring this keystone species.

In this study, we aim to refine the approach originally presented in McCarthy et al. (2023) to estimate GoM surface *C. finmarchicus* concentrations. We examine the applicability of this refined approach and explore factors influencing surface *C. finmarchicus* concentrations in the GoM as detected by ocean color remote sensing.

## 2 Materials and method

### 2.1 Satellite data and quality control

In this study, we used satellite data from MODIS Aqua (Moderate Resolution Imaging Spectroradiometer on the Aqua satellite), chosen for its consistent long-term data record. We acquired daily Level 2 MODIS Aqua remote sensing reflectance [ $R_{rs}(\lambda)$ ] data, with the 1-km resolution at nadir, from the National Aeronautics and Space Administration (NASA) Ocean Biology Distributed Active Archive Center (OB.DAAC; <https://oceancolor.gsfc.nasa.gov/>). We mapped each daily Level 2 scene employing the l2bin and l3magen tools available in the SeaDAS-OCSSW software version 8.3 (the NASA Ocean Biology Processing Group Science Software).

The GoM is an optically complex environment, and consequently, the atmospheric correction process can over-correct blue wavelengths, resulting in non-physical negative  $R_{rs}(\lambda)$  values or unrealistic spectral shapes. Thus, to ensure the quality of the  $R_{rs}(\lambda)$  dataset, we applied two quality control (QC) approaches. First, we removed all  $R_{rs}(\lambda)$  spectra that were negative at any wavelength. Second, we applied the Quality Water Index Polynomial (QWIP) method of Dierssen et al. (2022). QWIP is a quantitative metric approach and was developed to assess the quality of  $R_{rs}(\lambda)$  in the visible wavelength spectral range of 400–700 nm. The QWIP score is used to identify spectra that fall outside the general trends observed in aquatic optics for optically deep waters. For this study,  $R_{rs}(\lambda)$  spectra that fall outside the QWIP score of  $|0.2|$  were flagged to eliminate poorer quality spectra, as suggested by Dierssen et al. (2022).

### 2.2 eRGB image processing

The quality-controlled satellite  $R_{rs}(\lambda)$  were converted to enhanced RGB (eRGB) images using a standardized linear contrast image stretching method and gamma correction (McCarthy et al., 2023). Briefly, the eRGB image processing procedure standardizes the RGB bands by applying a standardized stretch technique and a gamma correction specifically for the blue band. The standardized stretch range had a minimum of zero and a maximum taken as the 90th percentile of each band in a global *in situ* dataset of  $R_{rs}(\lambda)$  (Valente et al., 2022). This approach was implemented to resolve visual inconsistencies between individual satellite images. When creating an RGB image, typically each color band is scaled based on the maximum and minimum values present in the given image, resulting in different scalings being used for each image (McCarthy et al., 2023). By standardizing the range over which each band is scaled, different images are directly comparable. This is crucial for accurate analysis and comparison of satellite data, especially when dealing with a large number of satellite images. Following McCarthy et al. (2023), we generated eRGB images using three  $R_{rs}(\lambda)$  wavebands from the quality-controlled satellite  $R_{rs}(\lambda)$  data: 443 nm for the blue channel, 488 nm for the green channel, and 555 nm for the red channel. This approach provides standardized eRGB data that are consistent across the whole dataset.

## 2.3 Continuous Plankton Recorder *C. finmarchicus* observations and satellite eRGB comparison

To verify the presence of surface patches in eRGB satellite imagery as *C. finmarchicus*, we utilized *in situ* abundance data of *C. finmarchicus* stage V–VI from the Continuous Plankton Recorder (CPR) collected in the GoM, sourced from a CPR database maintained by the National Oceanic and Atmospheric Administration (NOAA). The CPR is towed horizontally behind ships of opportunity, enabling continuous sampling of surface zooplankton (Richardson et al., 2006), making it an ideal dataset to compare with surface satellite observations. The CPR program has generated a long-term (1961–2013) and standardized database of marine zooplankton counts, which includes *C. finmarchicus* (Parent et al., 2012). The GoM CPR transect spans 450 km across the GoM, extending from Massachusetts to Nova Scotia in a west–east direction.

The initial identification of *C. finmarchicus* patches in eRGB satellite imagery involved comparing *in situ* CPR *C. finmarchicus* stage V–VI and eRGB satellite data from 2003 to 2013. We selected this timeframe due to the overlap of data availability from both CPR and MODIS Aqua satellite data. We focused initially on identifying high-abundance *C. finmarchicus* patches by selecting the highest 1% of the CPR values. From a dataset of 1,143 values, this resulted in 85 data points above a *C. finmarchicus* abundance of 10,000 individuals  $\text{m}^{-3}$  ( $\text{ind m}^{-3}$ ). We chose this threshold to enhance computational efficiency while ensuring the initial identification of *C. finmarchicus* presence. Based on the time and location of the top 1% *C. finmarchicus* abundance observations, we identified potential patches in the satellite eRGB imagery. We checked imagery from the same day of the CPR observation in the region surrounding the location of the observation.

## 2.4 Anomaly detection and estimation of surface *C. finmarchicus* abundance

In this study, we aim to refine the method presented by McCarry et al. (2023) to estimate the surface abundance of *C. finmarchicus*. This approach relies on satellite ocean color observations; thus, due to the diel vertical migration undergone by *C. finmarchicus*, the method presented provides a snapshot of the surface community in the middle of the day, rather than an estimate of the full community. Here, we give a brief overview of the McCarry et al. (2023) approach (which we denote as MC23 for brevity) and highlight the areas for refinement.

The core of the MC23 remote sensing method is based on two look-up tables (LUTs). These LUTs were created using a Case 2 (Morel and Prieur, 1977) bio-optical model based on Lo Prejato et al. (2020) and using specific inherent optical properties from Bengil et al. (2016) and Basedow et al. (2019). In the first LUT, referred to as the “Case 2” LUT, the bio-optical model contained the OSCs of phytoplankton chlorophyll-*a* and algal biogenic detritus (denoted as CHL), CDOM, and inorganic mineral suspended solids (MSS). The second LUT is the

same as the first, except that it includes *C. finmarchicus* and is referred to as the “Case 2 + *C. finmarchicus*” LUT. For each LUT, typical ranges of concentrations for each of the OSCs were used, and  $R_{rs}(\lambda)$  was calculated using the radiative transfer software EcoLight v5.3 (Mobley and Sundman, 2016). Finally,  $R_{rs}(\lambda)$  spectra were converted to eRGB values in the same manner as described above for the satellite data. Thus, the final LUTs contained OSC concentrations with corresponding eRGB values.

In MC23, for one eRGB satellite image, every pixel was compared with the eRGB values in the LUTs (Case 2 and Case 2 + *C. finmarchicus*). The comparison between the satellite and LUTs eRGB was quantified using the Delta E 2000 ( $\Delta E_{2000}$ ) algorithm, which is based on the CIE2000 model developed by the International Commission on Illumination (CIE).  $\Delta E_{2000}$  is a standard way of quantifying the difference between two colors in the  $L^* a^* b^*$  (where  $L^*$  = lightness,  $a^*$  = red–green axis, and  $b^*$  = yellow–blue axis) color space.  $\Delta E_{2000}$  values range from 0 to 100, where low  $\Delta E_{2000}$  value indicates that the two colors are similar, while a higher value indicates a high difference. Therefore, in this study and MC23, a “best match” between a satellite pixel and the LUT was taken as the lowest  $\Delta E_{2000}$  value ( $\Delta E_{2000}^{\text{min}}$ ). For a given satellite image, a map of  $\Delta E_{2000}^{\text{min}}$  acts as an anomaly map: low  $\Delta E_{2000}^{\text{min}}$  values indicate the satellite pixels are well described by the bio-optical model (i.e., there is a low anomaly between the bio-optical model and the satellite observation), and conversely, higher  $\Delta E_{2000}^{\text{min}}$  values indicate a less well described (more anomalous) system. MC23 showed that using the Case 2 + *C. finmarchicus* LUT reduced the anomaly (i.e., the  $\Delta E_{2000}^{\text{min}}$  values were lower) compared to the Case 2 LUT in a dense patch of *C. finmarchicus*. Further, the *C. finmarchicus* concentration was then estimated from the LUT value that corresponded to the  $\Delta E_{2000}^{\text{min}}$  for every pixel.

In this study, we used an updated version of the Case 2 + *C. finmarchicus* LUT from MC23, in which MSS values are varied, instead of the constant MSS value of  $0.03 \text{ g m}^{-3}$ . The updated version of the Case 2 + *C. finmarchicus* LUT has 4,410 entries, an increase from 1,176 entries (in MC23). In this paper, all future mentions of the Case 2 + *C. finmarchicus* LUT refer to this updated LUT (rather than the original in MC23). With a larger LUT, the process of comparing every pixel with every eRGB value in the LUT becomes computationally more expensive. In addition, there is the potential for even further increases in computational time and resources as we start to explore larger numbers of satellite images or create a finer-resolution LUT (i.e., more concentrations for the OSC). Thus, we explored the effectiveness of using a threshold-based approach. Here, we compared a given satellite image to the Case 2 LUT (which has a total of 1,008 entries, as in MC23). The  $\Delta E_{2000}^{\text{min}}$  anomaly map then highlights the regions where the Case 2 model does not sufficiently describe the system. However, where the anomaly is low, the Case 2 model is considered sufficient. Therefore, only pixels with a Case 2  $\Delta E_{2000}^{\text{min}}$  value exceeding the implemented threshold had the updated Case 2 + *C. finmarchicus* LUT applied. Thus, with this approach, we only applied the Case 2 + *C. finmarchicus* LUT to a subset of the pixels, not the whole image, and for those pixels, we were able to estimate the *C. finmarchicus* concentration based on the value from the LUT that corresponds to the  $\Delta E_{2000}^{\text{min}}$ , as in MC23.

## 3 Results

### 3.1 Detection of *C. finmarchicus* in eRGB imagery

We detected potential patches of *C. finmarchicus* in the eRGB imagery based on the highest 1% of the *C. finmarchicus* abundances in the CPR data. Figure 1 illustrates an example: the detection of a potential *C. finmarchicus* patch in eRGB imagery taken on June 17, 2009, identified through comparison with *in situ* CPR *C. finmarchicus* data. The eRGB image shows a region of red/brown pixels, potentially indicative of a *C. finmarchicus* patch (McCarry et al., 2023). The recorded CPR *C. finmarchicus* abundance at 19:33 local time (EST) was 21,402 ind m<sup>-3</sup> at the location depicted by a white star in Figure 1. Thus, the high CPR observation coincides with the potential patch of *C. finmarchicus* visible in the satellite imagery. The match between the eRGB satellite imagery and the CPR *C. finmarchicus* data provides evidence supporting the results of McCarry et al. (2023): dense patches of *C. finmarchicus* can be detected in eRGB imagery. Further, this demonstrates the applicability of the MC23 approach in a new region.

### 3.2 Threshold-based anomaly detection

To investigate the  $\Delta E_{2000}^{min}$  threshold limit to use for the threshold-based approach, we binned the Case 2  $\Delta E_{2000}^{min}$  values (see Figure 2). Different threshold values are used for defining a color difference (i.e., the  $\Delta E_{2000}$ ) depending on the application. In the printing industry, colors are considered visually consistent within a  $\Delta E_{2000}$  threshold of 4 (Liu et al., 2012). Therefore, to test this threshold for this particular application, we binned  $\Delta E_{2000}^{min}$  values of 0–4 within the first bin, and then we binned higher  $\Delta E_{2000}^{min}$  values in steps of 2.

In Figure 2, regions in the GoM and off the coast of Norway identified as potential *C. finmarchicus* patches show  $\Delta E_{2000}^{min}$  values larger than 4 (see Figure 1 and figure 10 of McCarry et al., 2023). These higher  $\Delta E_{2000}^{min}$  values indicate a greater deviation between the “best-matched” satellite and Case 2 LUT eRGB values. This deviation suggests that the pixels remain anomalous and are not optically resolved.

For the GoM image, we applied the Case 2 + *C. finmarchicus* LUT to the pixels where the Case 2  $\Delta E_{2000}^{min} \geq 4$ .

Figure 3 shows a refined version of the  $\Delta E_{2000}^{min}$  anomaly map, which combines  $\Delta E_{2000}^{min}$  values from the Case 2 LUT and the Case 2 + *C. finmarchicus* LUT. This refined binned  $\Delta E_{2000}^{min}$  anomaly map shows a lower  $\Delta E_{2000}^{min}$  across the entire image. The reduced  $\Delta E_{2000}^{min}$  values suggest that incorporating the *C. finmarchicus* component into the LUT resolved the anomalies in the regions where the Case 2  $\Delta E_{2000}^{min}$  values were  $\geq 4$ . Thus, the binned  $\Delta E_{2000}^{min}$  anomaly maps indicate that a Case 2  $\Delta E_{2000}^{min}$  threshold of  $\geq 4$  typically identifies pixels that are anomalous due to *C. finmarchicus*.

### 3.3 Surface *C. finmarchicus* concentration

Surface *C. finmarchicus* concentrations were quantified using the threshold-based approach, where each satellite pixel was first compared to the Case 2 LUT, and for any pixels where  $\Delta E_{2000}^{min}$  was above the threshold ( $\geq 4$ ), the Case 2 + *C. finmarchicus* LUT was used. The surface concentration of *C. finmarchicus* was then estimated only for those pixels where the Case 2 + *C. finmarchicus* LUT was used, and the *C. finmarchicus* concentration was taken from the combination of OSCs that produced the identified  $\Delta E_{2000}^{min}$  value. Using this approach on the MODIS Aqua eRGB imagery shown in Figure 1, Gulf-wide surface *C. finmarchicus* concentrations (Figure 4) were estimated, with peak concentrations of 150,000 ind m<sup>-3</sup> within the patch.

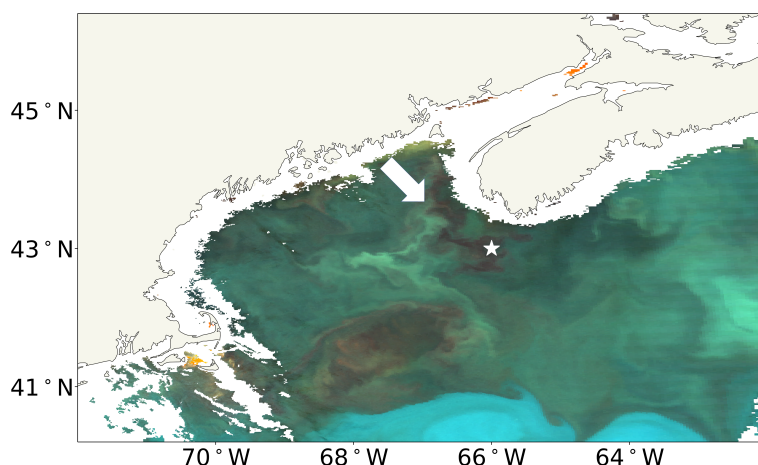


FIGURE 1

MODIS Aqua eRGB image of the GoM from June 17, 2009. The white star represents the *in situ* CPR observation with high *Calanus finmarchicus* abundance on the same day as the satellite image, and the white arrow points to the region of red/brown pixels indicative of a *C. finmarchicus* patch. eRGB, enhanced RGB; GoM, Gulf of Maine; CPR, Continuous Plankton Recorder.

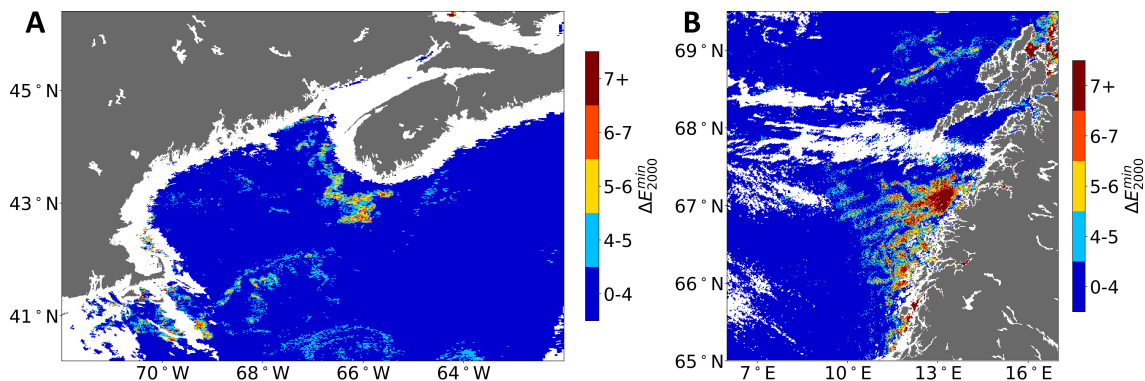


FIGURE 2

Binned  $\Delta E_{2000}^{min}$  Case 2 anomaly map of (A) GoM (same image as shown in Figure 1); (B) off the coast of Norway (same image used in McCarry et al., 2023). GoM, Gulf of Maine.

### 3.4 Factors affecting the estimation of surface *C. finmarchicus* abundance

The GoM is known to have a wide variety of zooplankton species, many of which have the pigment astaxanthin, for example, *Centropages* and krill (Bandaranayake and Gentien, 1982; Koomyart et al., 2017). As the MC23 method is based on the detection of astaxanthin, other astaxanthin or red-colored species may mistakenly be detected as *C. finmarchicus*. To explore this potential misidentification, we examined satellite images at times of the year when *C. finmarchicus* is not typically present in the surface waters of the GoM but other astaxanthin or red-colored species are. Here, we present two case studies, highlighting the effect on *C. finmarchicus* abundance estimates from other astaxanthin or red-colored species.

In the first case, we observed an apparent high abundance of surface *C. finmarchicus* in the late fall, as shown in Figure 5. Typically, *C. finmarchicus* is expected to be in diapause in the late fall; thus, it is less likely they will be present in surface waters (Häfker et al., 2018). In this case, the Case 2  $\Delta E_{2000}^{min}$  anomaly map (see Figure 5B) shows high  $\Delta E_{2000}^{min}$  values across much of the region. The refined  $\Delta E_{2000}^{min}$  map shows low  $\Delta E_{2000}^{min}$  values in these anomalous regions, indicating that these pixels appear to be well resolved by the Case 2 + *C. finmarchicus* LUT

(Figure 5C). The estimated surface *C. finmarchicus* concentration (see Figure 5D) corresponding to the refined  $\Delta E_{2000}^{min}$  anomaly map is high in these regions that were anomalous when using the Case 2 LUT only, but not when using the Case 2 + *C. finmarchicus* LUT. In this case, local knowledge suggests that it is less likely to be *C. finmarchicus* present at the surface during late fall and more likely to be *Centropages*, a species known to be in the surface waters of the GoM in November (Stegert et al., 2012). If so, this set of results could indicate that the  $\Delta E_{2000}^{min}$  anomaly method identifies astaxanthin pigment, irrespective of species, and the high surface concentrations of *C. finmarchicus* estimated during the late fall may actually be attributed to other astaxanthin containing zooplankton species.

The second case study illustrates how dark red/brown phytoplankton blooms may be misidentified as *C. finmarchicus*. There was a large bloom of *Tripes muelleri*, a brown dinoflagellate, in the GoM in the spring and summer of 2023 (Ray, 2023). Thus, to explore the impact of a different red/brown organism on this ocean color remote sensing approach, a single scene from spring 2023 was acquired and processed in the same way as previously described (Figure 6). In this case, the anomalous pixels in the Case 2  $\Delta E_{2000}^{min}$  anomaly map are high and extensive across the GoM (Figure 6B). While the  $\Delta E_{2000}^{min}$  anomaly is reduced using the refined, threshold-

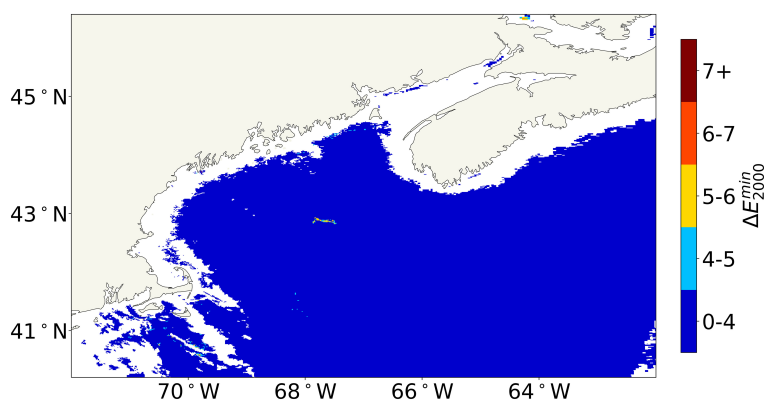


FIGURE 3

Same as Figure 2A, except that the Case 2 + *Calanus finmarchicus* LUT was applied to the pixels where the Case 2  $\Delta E_{2000}^{min} \geq 4$ . LUT, look-up table.

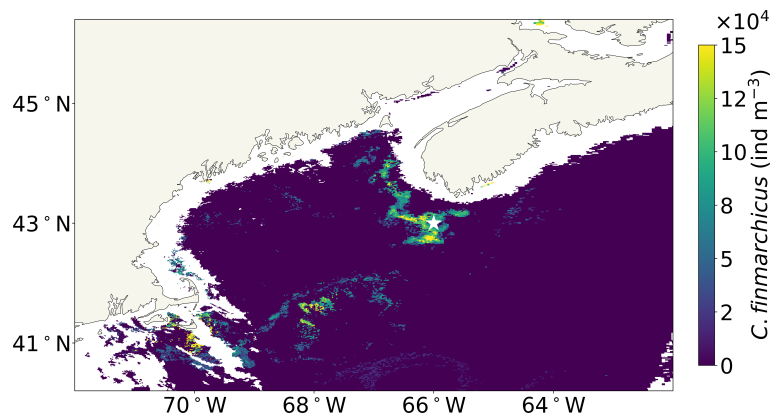


FIGURE 4

Surface concentrations of *Calanus finmarchicus* in the GoM estimated using the threshold-based approach on June 17, 2009, with the star indicating the location of the *in situ* CPR observation. GoM, Gulf of Maine; CPR, Continuous Plankton Recorder.

based approach (see Figure 6C), the anomalies are still high. The presence of anomalous pixels in the refined  $\Delta E_{2000}^{min}$  anomaly map indicates that the pixels are not well resolved by the Case 2 + *C. finmarchicus* LUT; i.e., the addition of *C. finmarchicus* did not fully remove the anomaly. The estimated surface *C. finmarchicus* concentration (see Figure 6D) is high across the GoM. When *C. finmarchicus* swarm at the surface, they tend to be in small patches, and the Gulf-wide feature in Figure 6D is unusual. Therefore, the unresolved refined  $\Delta E_{2000}^{min}$  anomaly (Figure 6C), the spatial extent of the *C. finmarchicus* patch, and the known presence of *T. muelleri* suggest a misidentification *C. finmarchicus*.

## 4 Discussion

### 4.1 *C. finmarchicus* detection through eRGB image processing

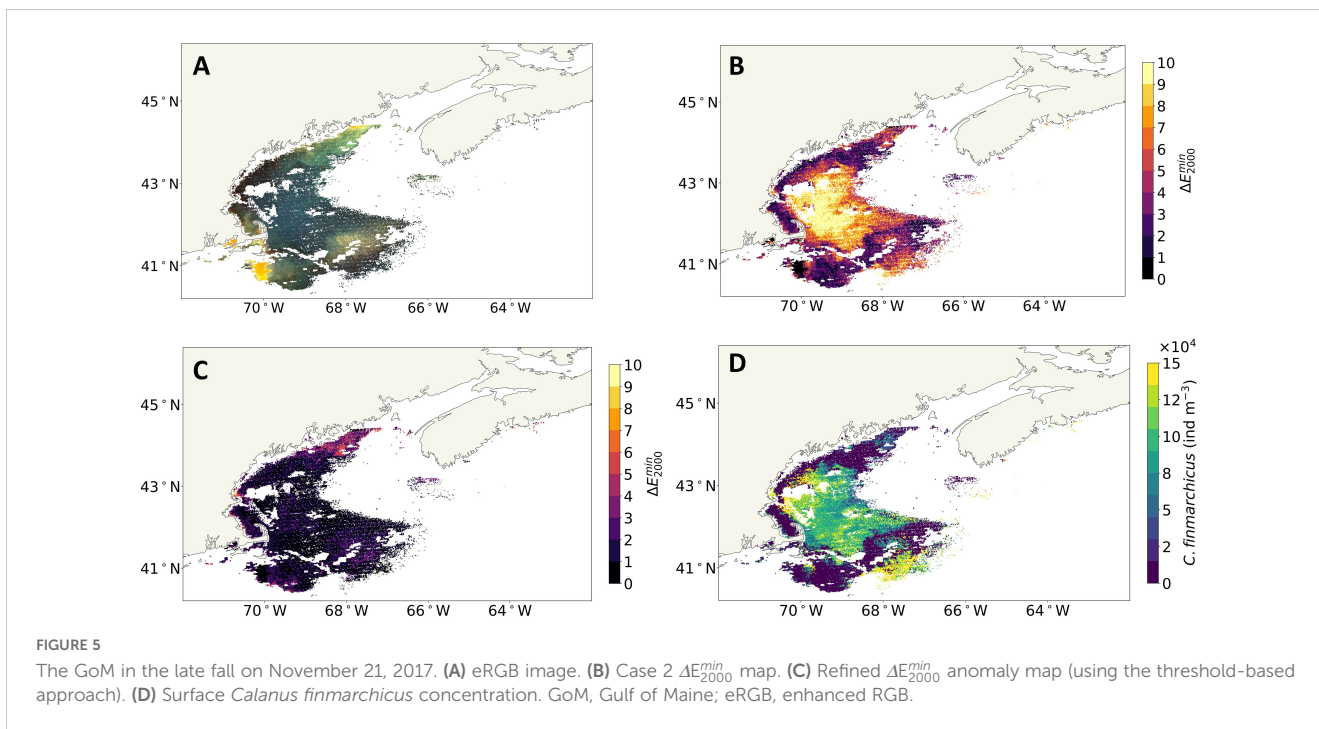
We applied the eRGB image processing technique from MC23 to identify potential patches of surface *C. finmarchicus* in the GoM. While the eRGB standardization technique developed by McCarry et al. (2023) was initially intended for the Norwegian Sea, the range was derived from a comprehensive global dataset (Valente et al., 2022). Thus, the direct application of the MC23 eRGB approach is equally effective in standardizing satellite RGBs for the GoM. The implementation of the eRGB image standardizing technique is particularly crucial when working with large time-scale datasets, as it ensures consistency across the eRGB images, thereby allowing direct comparison between them.

### 4.2 Optical anomaly detection for estimating surface *C. finmarchicus* in the GoM

The anomaly detection process is a test of optical closure. The refined anomaly detection used a threshold-based approach, where a Case 2  $\Delta E_{2000}^{min} \geq 4$  was identified as anomalous (see Figure 2). In

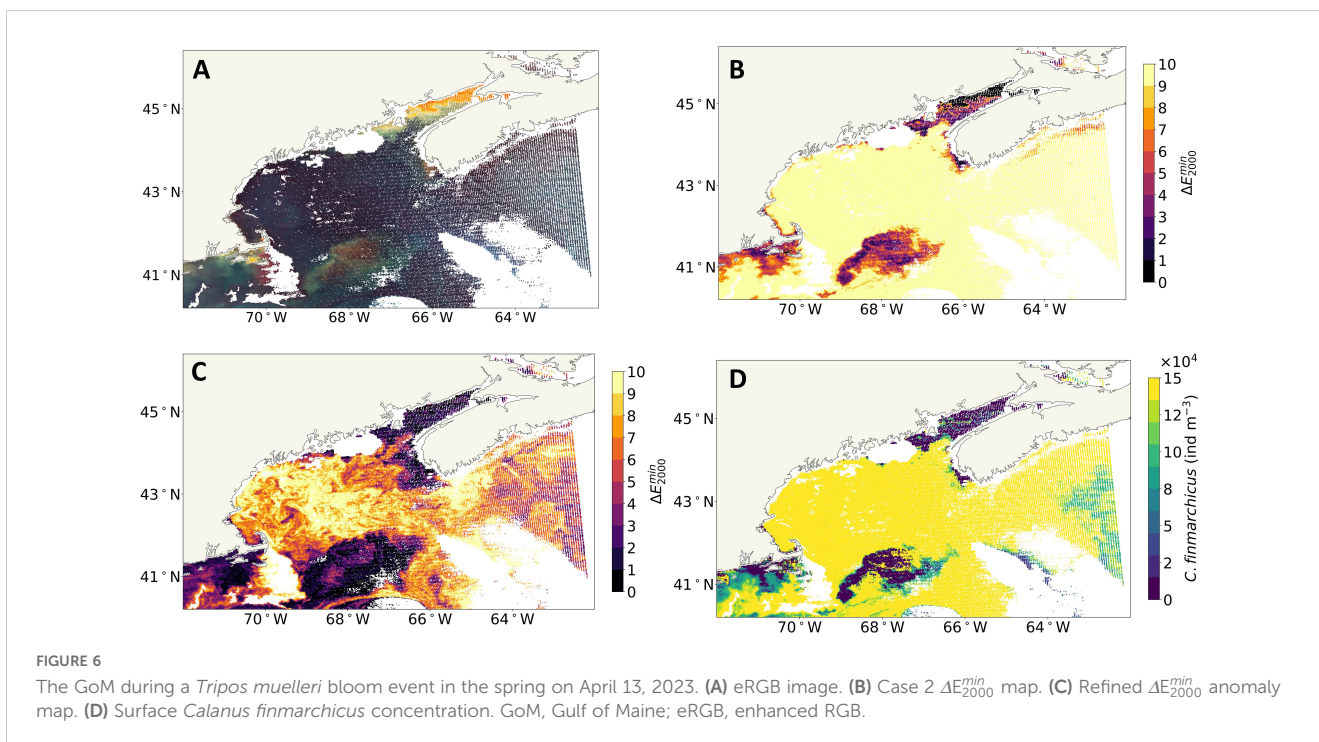
the case of the June 2009 image (Figures 2A, 3), we observed high  $\Delta E_{2000}^{min}$  values ( $\geq 4$ ) in the Case 2  $\Delta E_{2000}^{min}$  anomaly map (Figure 2A), particularly in regions of potential *C. finmarchicus*. This suggests that the Case 2 bio-optical model in these areas is incomplete, and the potential *C. finmarchicus* patch is anomalous without the inclusion of the *C. finmarchicus* constituent. In the refined, threshold-based approach, the Case 2 + *C. finmarchicus* LUT was applied on the anomalous pixels, resulting in significantly lower  $\Delta E_{2000}^{min}$  values, indicating that the anomaly in the optical model was resolved with the addition of *C. finmarchicus* (Figure 3). Therefore, in this case, the addition of *C. finmarchicus* component into the Case 2 standard bio-optical model in the anomalous region resolves the anomalies between the bio-optical model and the satellite imagery, as evidenced by the lower  $\Delta E_{2000}^{min}$  values in the refined  $\Delta E_{2000}^{min}$  anomaly.

Both case studies, illustrated in Figures 5, 6, highlight factors that impact the accuracy of the ocean color anomaly detection method for estimating *C. finmarchicus* concentrations. The method presented here, and in McCarry et al. (2023), relied on the detection of astaxanthin to quantify *C. finmarchicus*. Astaxanthin is a pigment common in various zooplankton species, and there are red/brown phytoplankton species, with many of these plankton and phytoplankton species present in the GoM. We found an unusually high *C. finmarchicus* concentration in late fall, which is likely to be another astaxanthin-rich species such as *Centropages*. Furthermore, a bloom of *T. muelleri* was misidentified as a large swarm of *C. finmarchicus*. These instances suggest that the method can be used to detect the presence of red/brown/astaxanthin-rich species, but without *a priori* knowledge of the system, a specific species cannot be identified. In the case of the *T. muelleri* bloom, the anomalous pixels in the refined anomaly map (high  $\Delta E_{2000}^{min}$  values in Figure 6C) indicate that the Case 2 + *C. finmarchicus* LUT did not fully resolve the anomaly. This, along with the estimation of high *C. finmarchicus* concentrations (concentrations at the maximum value included in the LUT, see Figure 6D), suggests that even higher concentrations of *C. finmarchicus* are needed in the LUT to resolve the anomaly.



Alternatively, the failure to eliminate the anomaly using the existing *C. finmarchicus* range in the LUT could be used to identify a further mismatch, and therefore, the resulting *C. finmarchicus* estimates could be eliminated as being unrealistic. Here, we estimated *C. finmarchicus* concentrations (in individuals  $m^{-3}$ ) based on the absorption coefficient for individual *C. finmarchicus*. However, other red/brown/astaxanthin-rich plankton package their pigments differently,

and therefore, each species will absorb different amounts per individual. Thus, the *C. finmarchicus* concentrations shown in Figures 5D, 6D cannot simply be taken as concentrations of *Centropages* or *T. muelleri*, and appropriate species and pigment-specific absorption measurements are required. This package effect is likely to happen within a given species, related to the size of the individuals, stage of life cycle, or physiological effects; thus, the variability in species-specific absorption also



needs to be quantified. Consequently, we conclude that the refined, threshold-based anomaly detection method has the potential for detecting surface astaxanthin-rich or red-colored species. These could then be converted to species concentration with local knowledge of the species present and an appropriate, species-specific absorption measurement. To obtain species-specific absorption, it is important to measure the *in situ* absorption of astaxanthin-rich zooplankton under varying conditions, including different locations, life stages, and concentrations.

Optical closure may fail because either there is a problem in our bio-optical model or because there is an issue with the satellite data. Given the optically complex nature of the GoM, there can be issues with the atmospheric correction, particularly near the coast. While we have implemented a QC approach to remove spectra that have atmospheric correction issues, it is likely this approach is not perfect. The bio-optical model we used was built from Ligurian Sea data, and its application in the GoM may have caused misclassifications, although we are encouraged by the degree of optical closure that has been achieved. Implementing a GoM bio-optical model (including additional OSCs) and improving satellite atmospheric correction may further improve optical closure and the accuracy in identifying and quantifying *C. finmarchicus* for this region.

### 4.3 Difference between *in situ* and satellite *C. finmarchicus* estimation

The *in situ* CPR *C. finmarchicus* population in the GoM recorded at approximately 19:33 local time (EST) on June 17, 2009, was 21,402 ind m<sup>-3</sup> at the location depicted by a white star in Figures 1, 4. The refined anomaly detection method estimated the surface concentration of *C. finmarchicus* at the same location to be 80,000 ind m<sup>-3</sup>, obtained from satellite imagery captured earlier that day at 13:12 local time (EST). Although these *in situ* and satellite measurements were taken at different times on the same day, other factors contributing to this discrepancy should also be considered. However, the discrepancy between *in situ* and satellite measurements is consistent with the findings of McCarry et al. (2023). A potential factor for the discrepancy between satellite and *in situ* data could be partially attributed to the self-propelling movement of *C. finmarchicus*. Some studies have shown the ability of *C. finmarchicus* to avoid capture in net sampling, highlighting factors that contribute to the underestimation of population densities, including copepods' ability to detect nets in daylight and their tendency to avoid them (Fleminger and Clutter, 1965; Giering et al., 2022). This behavior, often linked to their sensitivity to the noise and disturbances created by ship movements and the CPR sampling process, could lead to a significant underestimation of their true population numbers. Furthermore, a comparative study by Baumgartner (2003) on *C. finmarchicus* abundance estimates, utilizing net samples and optical plankton counters in the GoM, revealed that in patchy distribution

environments, substantial concentrations of *C. finmarchicus* may not be adequately captured by nets, CPR, or instruments. It has also been shown that the CPR in particular tends to underestimate zooplankton populations due to its small aperture, which makes evasion relatively easy (Dippner and Krause, 2013). Further, the *in situ* CPR data only include stages V and VI *C. finmarchicus*, whereas the satellite measurements will include all life stages that contain astaxanthin. Consequently, the *in situ* values would be lower than the satellite estimates, as seen in our results. Collectively, these insights underline the complexities in accurately gauging the population densities of such copepods. The limitations inherent in both traditional zooplankton nets and optical plankton counters pose challenges for ecological modeling like NARW modeling, which depends on these data sources. However, for modeling NARW populations, thresholds of *C. finmarchicus* concentration become important. Ross et al. (2023) found that *C. finmarchicus* concentrations exceeding 10,000 ind m<sup>-3</sup> are indicative of NARW presence. Further, McCarry et al. (2024) found that the minimum detectable level of *C. finmarchicus* via the MC23 approach was 1,300 ind m<sup>-3</sup> in Case 1 waters and 8,700 ind m<sup>-3</sup> in Case 2 waters. Given the potential for underestimation by *in situ* sampling techniques, it is likely that the Ross et al. threshold would translate into an even larger number for remote sensing observation. Thus, in the optically complex, Case 2 waters of the GoM, the minimum detectable *C. finmarchicus* concentration from the satellite is worse than the concentration indicative of NARW presence and may in fact be significantly lower.

### 4.4 Future considerations for ocean color anomaly detection for quantifying surface *C. finmarchicus* concentrations

One potential way to improve the *C. finmarchicus* quantification would be adopting a spectral matching approach that utilizes the full spectral signatures, moving beyond the three RGB bands used here. This solution, however, has challenges set by the limited availability of spectral bands on heritage ocean color satellites (SeaWiFS, MODIS, and VIIRS) that are capable of effectively differentiating spectral signatures between these species. The new NASA PACE mission will provide global-scale hyperspectral data and could consequently enhance methods for quantifying *C. finmarchicus* and other optically significant zooplankton. The spectral differences in zooplankton due to different pigments could be detectable via PACE due to its higher spectral resolution; however, McCarry et al. (2024) found that reflectance spectra from astaxanthin-rich and non-astaxanthin-rich zooplankton were similar. Nevertheless, there only exist a limited number of measurements of zooplankton optical properties. Thus, more *in situ* measurements of zooplankton optical properties, coupled with *in situ* measurements of zooplankton concentrations (ideally from multiple sampling approaches, e.g., nets, optical plankton counters, and acoustics), are important for developing and refining approaches for ocean color-based zooplankton detection.

The bio-optical model used in this study did not include a component for the backscattering coefficient of *C. finmarchicus*. Although the backscattering signal of *C. finmarchicus* is likely minimal and deemed negligible due to their larger particle size (Davies et al., 2021), the development of an instrument to measure large particle backscattering would help to measure the backscattering component, thus potentially enhancing the accuracy of the *C. finmarchicus* bio-optical model. Additionally, considering the varying concentrations of astaxanthin pigment in different astaxanthin-rich species, which affect their absorption and backscattering properties, and understanding the species-specific astaxanthin pigment concentration could help to differentiate these species and improve the accuracy of species concentration estimates. Thus, it is important to build up a database of *in situ* zooplankton absorption measurements and quantify the variability in these observations.

## 5 Conclusion

This study highlights the potential of ocean color remote sensing and bio-optical modeling in detecting surface concentrations of *C. finmarchicus* in the GoM and underscores the importance of considering zooplankton when evaluating the optical properties of ocean waters. However, the approach presented here also detects other astaxanthin/red-colored species and misidentifies them as *C. finmarchicus* because they are optically indistinguishable from each other. Thus, this approach is effectively an astaxanthin/red detection method, and rather than estimating concentrations of a given species, producing an estimate of astaxanthin concentration that could subsequently be converted into an equivalent species abundance would provide a more universally applicable output. That being said, with local knowledge and species-specific absorption coefficients, surface concentrations of a given species can be estimated (as was shown here). Consequently, surface detection of astaxanthin-rich plankton using ocean color remote sensing holds promise for many applications, including tracking changes in NARW migration by leveraging satellite-based estimates of surface *C. finmarchicus* concentration patterns.

## Data availability statement

The original contributions presented in the study are included in the article/supplementary material. Further inquiries can be directed to the corresponding author.

## References

Bandaranayake, W. M., and Gentien, P. (1982). Carotenoids of *temora turbinata*, *centropages furcatus*, *undinula vulgaris* and *euchaeta russelli*. *Comp. Biochem. Physiol. Part B: Comp. Biochem.* 72, 409–145. doi: 10.1016/0305-0491(82)90219-X

## Author contributions

RS: Data curation, Formal Analysis, Investigation, Visualization, Writing – original draft, Writing – review & editing. CLM: Methodology, Writing – review & editing, Resources. DM: Conceptualization, Methodology, Writing – review & editing. CM: Conceptualization, Funding acquisition, Supervision, Writing – review & editing.

## Funding

The author(s) declare that financial support was received for the research, authorship, and/or publication of this article. This research was funded by the NASA (National Aeronautics and Space Administration) grant number 80NSSC21K1733, Norges Forskningsråd (287043 STRESSOR project), and Natural Environment Research Council (NE/Y004426/1).

## Acknowledgments

The authors would like to thank the NASA OBPG/OB.DAAC for the open-source satellite data and the National Oceanic and Atmospheric Administration (NOAA) for the CPR data source.

## Conflict of interest

The authors declare that the research was conducted in the absence of any commercial or financial relationships that could be construed as a potential conflict of interest.

## Generative AI statement

The author(s) declare that no Generative AI was used in the creation of this manuscript.

## Publisher's note

All claims expressed in this article are solely those of the authors and do not necessarily represent those of their affiliated organizations, or those of the publisher, the editors and the reviewers. Any product that may be evaluated in this article, or claim that may be made by its manufacturer, is not guaranteed or endorsed by the publisher.

Basedow, S.L., McKee, D., Lefering, I., Gislason, A., Daase, M., Trudnowska, E., et al. (2019). Remote sensing of zooplankton swarms. *Sci. Rep.* 9, 6865. doi: 10.1038/s41598-018-37129-x

- Baumgartner, M. F. (2003). Comparisons of calanus finmarchicus fifth copepodite abundance estimates from nets and an optical plankton counter. *J. Plankton Res.* 25, 855–868. doi: 10.1093/plankt/25.7.855
- Bengil, F., McKee, D., Beşiktepe, S. T., Calzado, V. S., and Trees, C. (2016). A bio-optical model for integration into ecosystem models for the ligurian sea. *Prog. Oceanography* 149, 1–15. doi: 10.1016/j.pocean.2016.10.007
- Bigelow, H. B. (1926). *Plankton of the Offshore Waters of the Gulf of Maine* (Washington: Govt. Print. Off). doi: 10.5962/bhl.title.4192
- Byron, E. R. (1982). The adaptive significance of calanoid copepod pigmentation: A comparative and experimental analysis. *Ecology* 63, 1871. doi: 10.2307/1940127
- Davies, E. J., Basedow, S. L., and McKee, D. (2021). The hidden influence of large particles on ocean colour. *Sci. Rep.* 11, 39995. doi: 10.1038/s41598-021-83610-5
- Dierssen, H. M., and Randolph, K. (2013). “Remote Sensing of Ocean Color,” in *Earth System Monitoring*. Ed. J. Orcutt (Springer New York, New York, NY), 439–472. doi: 10.1007/978-1-4614-5684-1\_18
- Dierssen, H. M., Vandermeulen, R. A., Barnes, B. B., Castagna, A., Knaeps, E., and Vanhellemont, Q. (2022). QWIP: A quantitative metric for quality control of aquatic reflectance spectral shape using the apparent visible wavelength. *Front. Remote Sens.* 3. doi: 10.3389/frsen.2022.869611
- Dippner, J. W., and Krause, M. (2013). Continuous plankton recorder underestimates zooplankton abundance. *J. Mar. Syst.* 111–112, 263–268. doi: 10.1016/j.jmarsys.2012.09.009
- Fleminger, A., and Clutter, R. I. (1965). AVOIDANCE OF TOWED NETS BY ZOOPLANKTON. *Limnology Oceanography* 10, 96–1045. doi: 10.4319/lo.1965.10.1.0096
- Giering, S. L. C., Culverhouse, P. F., Johns, D. G., McQuatters-Gollop, A., and Pitois, S. G. (2022). Are plankton nets a thing of the past? An assessment of in situ imaging of zooplankton for large-scale ecosystem assessment and policy decision-making. *Front. Mar. Sci.* 9. doi: 10.3389/fmars.2022.986206
- Grieve, B. D., Hare, J. A., and Saba, V. S. (2017). Projecting the effects of climate change on calanus finmarchicus distribution within the U.S. Northeast continental shelf. *Sci. Rep.* 7, 62645. doi: 10.1038/s41598-017-06524-1
- Groom, S., Sathyendranath, S., Ban, Y., Bernard, S., Brewin, R., Brotas, V., et al. (2019). Satellite ocean colour: current status and future perspective. *Front. Mar. Sci.* 6. doi: 10.3389/fmars.2019.00485
- Häfker, N. S., Teschke, M., Last, K. S., Pond, D. W., Hüppe, L., and Meyer, B. (2018). *Calanus finmarchicus* seasonal cycle and diapause in relation to gene expression, physiology, and endogenous clocks. *Limnology Oceanography* 63, 2815–2885. doi: 10.1002/lno.11011
- Ji, R., Runge, J. A., Davis, C. S., and Wiebe, P. H. (2022). Drivers of variability of calanus finmarchicus in the gulf of maine: roles of internal production and external exchange. *ICES J. Mar. Sci.* 79, 775–845. doi: 10.1093/icesjms/fsab147
- Johnson, C. L., Runge, J. A., Curtis, K. A., Durbin, E. G., Hare, J. A., Incze, L. S., et al. (2011). Biodiversity and ecosystem function in the gulf of maine: pattern and role of zooplankton and pelagic nekton. *PLoS One* 6, e164915. doi: 10.1371/journal.pone.0016491
- Koomyart, I., Nagamizu, H., Khuwijitjaru, P., Kobayashi, T., Shiga, H., Yoshii, H., et al. (2017). Astaxanthin stability and color change of krill during subcritical water treatment. *J. Food Sci. Technol.* 54, 3065–3725. doi: 10.1007/s13197-017-2742-1
- Liu, H. X., Wu, B., Liu, Y., Huang, M., and Xu, Y. F. (2012). A discussion on printing color difference tolerance by CIEDE2000 color difference formula. *Appl. Mechanics Materials* 262, 96–99. doi: 10.4028/www.scientific.net/AMM.262.96
- Lo Prejato, M., McKee, D., and Mitchell, C. (2020). Inherent optical properties-reflectance relationships revisited. *J. Geophysical Research: Oceans* 125, e2020J0016661. doi: 10.1029/2020J0016661
- Mascarenhas, V., and Keck, T. (2018). “Marine Optics and Ocean Color Remote Sensing,” in *YOU MARES 8 – Oceans Across Boundaries: Learning from Each Other*. Eds. S. Jungblut, V. Liebich and M. Bode (Springer International Publishing, Cham), 41–54. doi: 10.1007/978-3-319-93284-2\_4
- Matsuno, T. (2001). Aquatic animal carotenoids. *Fisheries Sci.* 67, 771–783. doi: 10.1046/j.1444-2906.2001.00323.x
- McCarthy, C. L., Basedow, S. L., Davies, E. J., Last, K. S., and McKee, D. (2024). Determination of zooplankton absorption spectra and their potential contribution to ocean color. *Optics Express* 32, 413145. doi: 10.1364/OE.537062
- McCarthy, C. L., Basedow, S. L., Davies, E. J., and McKee, D. (2023). Estimating surface concentrations of calanus finmarchicus using standardised satellite-derived enhanced RGB imagery. *Remote Sens.* 15, 29875. doi: 10.3390/rs15122987
- Melle, W., Runge, J., Head, E., Plourde, S., Castellani, C., Licandro, P., et al. (2014). The north atlantic ocean as habitat for calanus finmarchicus: environmental factors and life history traits. *Prog. Oceanography* 129, 244–284. doi: 10.1016/j.pocean.2014.04.026
- Meyer-Gutbrod, E., Greene, C., Davies, K., and Johns, D. (2021). Ocean regime shift is driving collapse of the north atlantic right whale population. *Oceanography* 34, 22–315. doi: 10.5670/oceanog.2021.308
- Michaud, J., and Taggart, C. (2007). Lipid and gross energy content of north atlantic right whale, *Calanus finmarchicus*, in the bay of fundy. *Endangered Species Res.* 3, 77–94. doi: 10.3354/esr003077
- Mobley, C. D., and Sundman, L. K. (2016). *HydroLight-EcoLight 5.3* (Sequoia Scientific Inc., Bellevue, DC, USA: Numerical Optics Ltd.).
- Moore, M. J., Rowles, T. K., Fauquier, D. A., Baker, J. D., Biedron, I., Durban, J. W., et al. (2021). REVIEW assessing north atlantic right whale health: threats, and development of tools critical for conservation of the species. *Dis. Aquat. Organisms* 143, 205–226. doi: 10.3354/dao03578
- Morel, A., and Prieur, L. (1977). Analysis of variations in ocean color. *Limnology Oceanography* 22, 709–225. doi: 10.4319/lo.1977.22.4.0709
- Parent, G. J., Plourde, S., and Turgeon, J. (2012). Natural hybridization between calanus finmarchicus and *C. glacialis* (Copepoda) in the arctic and northwest atlantic. *Limnology Oceanography* 57, 1057–1665. doi: 10.4319/lo.2012.57.4.1057
- Ray, R. (2023). *Researchers identify unusually large bloom of brown algae in the Gulf of Maine*. Available online at: <https://www.unh.edu/unhoday/news/release/2023/08/23/researchers-identify-unusually-large-bloom-brown-algae-gulf-maine>.
- Record, N., Runge, J., Pendleton, D., Balch, W., Davies, K., Pershing, A., et al. (2019). Rapid climate-driven circulation changes threaten conservation of endangered north atlantic right whales. *Oceanography* 32, 162–169. doi: 10.5670/oceanog.2019.201
- Renaud, P. E., Daase, M., Banas, N. S., Gabrielsen, T. M., Søreide, J. E., Varpe, Ø., et al. (2018). Pelagic food-webs in a changing arctic: A trait-based perspective suggests a mode of resilience. *ICES J. Mar. Sci.* 75, 1871–1881. doi: 10.1093/icesjms/isy063
- Richardson, A. J., Walne, A. W., John, A. W. G., Jonas, T. D., Lindley, J. A., Sims, D. W., et al. (2006). Using continuous plankton recorder data. *Prog. Oceanography* 68, 27–74. doi: 10.1016/j.pocean.2005.09.011
- Ross, C. H., Runge, J. A., Roberts, J. J., Brady, D. C., Tupper, B., and Record, N. R. (2023). Estimating north atlantic right whale prey based on calanus finmarchicus thresholds. *Mar. Ecol. Prog. Ser.* 703, 1–16. doi: 10.3354/meps14204
- Sorochan, K. A., Plourde, S., Baumgartner, M. F., and Johnson, C. L. (2021). Availability, supply, and aggregation of prey (*Calanus* spp.) in foraging areas of the north atlantic right whale (*Eubalaena glacialis*). *ICES J. Mar. Sci.* 78, 3498–3520. doi: 10.1093/icesjms/fsab200
- Stegert, C., Ji, R., Li, N., and Davis, C. S. (2012). Processes controlling seasonality and spatial distribution of centropages typicus: A modeling study in the gulf of maine/georges bank region. *J. Plankton Res.* 34, 18–35. doi: 10.1093/plankt/fbr084
- Swaim, Z. T., Westgate, A. J., Koopman, H. N., Rolland, R. M., and Kraus, S. D. (2009). Metabolism of ingested lipids by north atlantic right whales. *Endangered Species Res.* 6, 259–271. doi: 10.3354/esr00163
- Valente, A., Sathyendranath, S., Brotas, V., Groom, S., Grant, M., Jackson, T., et al. (2022). A compilation of global bio-optical in situ data for ocean colour satellite applications – version three. *Earth System Sci. Data* 14, 5737–5770. doi: 10.5194/essd-14-5737-2022
- Vilgrain, L., Maps, F., Basedow, S., Trudnowska, E., Madoui, M. -A., Niehoff, B., et al. (2023). Copepods’ True colors: astaxanthin pigmentation as an indicator of fitness. *Ecosphere* 14, e44895. doi: 10.1002/ecs2.4489
- Werdell, P. J., McKinna, L. I. W., Boss, E., Ackleson, S. G., Craig, S. E., Gregg, W. W., et al. (2018). An overview of approaches and challenges for retrieving marine inherent optical properties from ocean color remote sensing. *Prog. Oceanography* 160, 186–212. doi: 10.1016/j.pocean.2018.01.001